DOI: 10.1002/chem.200600453

Ligand Topology Effects on Olefin Oxidations by Bio-Inspired [$Fe^{II}(N_2Py_2)$] Catalysts

Rubén Mas-Ballesté,[a] Miquel Costas,[a, b] Tieme van den Berg,[a] and Lawrence Que, Jr.*[a]

Abstract: Linear tetradentate N_2Py_2 ligands can coordinate to an octahedral Fe^{II} center in three possible topologies (*cis*-α, *cis*-β, and *trans*). While for the *N,N′*-bis(2-pyridylmethyl)-1,2-diaminoethane (bpmen) complex, only the *cis*-α topology has been observed, for *N,N′*-bis(2-pyridylmethyl)-1,2-diaminocyclohexane (bpmcn) both *cis*-α and *cis*-β isomers have been reported. To date, no facile interconversion between *cis*-α and *cis*-β topologies has been observed for iron(II) complexes even at high temperatures. However, this work provides evidence for facile interconversion in solution of *cis*-α, *cis*-β, and *trans* topologies for [Fe(bpmpn)X_2] (bpmpn = *N,N′*-bis(2-pyridylmethyl)-1,3-diaminopropane; X = triflate, CH_3CN) complexes. As reported previously, the catalytic behavior of *cis*-α and *cis*-β isomers of [Fe(bpmcn)$(OTf)_2$] with respect to olefin oxidation depends dramatically on the geometry adopted by the iron complex. To establish a general pattern of the catalysis/topology dependence, this work presents an extended comparison of the catalytic behavior for oxidation of olefins of a family of [$Fe(N_2py_2)$] complexes that present different topologies. ^{18}O labeling experiments provide evidence for a complex mechanistic landscape in which several pathways should be considered. Complexes with a *trans* topology catalyze only non-water-assisted epoxidation. In contrast, complexes with a *cis*-α topology, such as [Fe(bpmen)X_2] and [Fe(α-bpmcn)$(OTf)_2$], can catalyze both epoxidation and *cis*-dihydroxylation through a water-assisted mechanism. Surprisingly, [Fe(bpmpn)X_2] and [Fe(β-bpmcn)$(OTf)_2$] catalyze epoxidation via a water-assisted pathway and *cis*-dihydroxylation via a non-water-assisted mechanism, a result that requires two independent and distinct oxidants.

Keywords: bio-inspired catalysis · hydrogen peroxide · iron · N ligands · olefin oxidation

Introduction

Many iron enzymes activate dioxygen and catalyze the stereospecific oxidation of C–H or C=C bonds.[1,2] Prominent among these are the cytochromes P450,[3,4] which participate in many important metabolic transformations and thus have been the subject of intense study. The cytochrome P450 active site has a mononuclear iron center that is coordinated to a porphyrin cofactor and is attached to the polypeptide chain with an axial cysteinate ligand.[5] Much effort has been invested in developing biomimetic iron porphyrin catalysts for substrate oxidation.[6,7] More recently, nonheme iron enzymes have become better characterized and been found to carry out similar transformations.[1,8] A particularly interesting class of nonheme iron enzymes are the Rieske dioxygenases that are responsible for the *cis*-dihydroxylation of arene double bonds, the first step in the biodegradation of arenes in the environment.[9,10,11,12] The *cis*-dihydroxylating active site of the Rieske dioxygenases consists of a mononuclear iron center that is coordinated to two histidines and a bidentate aspartate,[9] in a variation of the so-called 2-His-1-carboxylate facial triad.[13] This coordination environment leaves two adjacent sites available for exogenous ligand binding and indeed allows dioxygen to bind in a side-on mode,[10] which presumably activates it for the *cis*-dihydroxylation reaction. We have embarked on an effort to develop biomimetic catalysts inspired by the Rieske dioxygenases and discovered a family of nonheme iron complexes of tet-

[a] Dr. R. Mas-Ballesté, Dr. M. Costas, T. van den Berg, Prof. Dr. L. Que, Jr.
Department of Chemistry and Center for Metals in Biocatalysis
University of Minnesota
207 Pleasant St. SE, Minneapolis, MN 55455 (USA)
Fax: (+1) 612-624-7029
E-mail: que@chem.umn.edu

[b] Dr. M. Costas
Current address: Departament de Quimica, Universitat de Girona, 17071, Girona (Spain)

radentate N4 ligands that use H_2O_2 efficiently as oxidant for highly stereoselective oxidations of olefins.[14,15] Both olefin epoxidation and *cis*-dihydroxylation reactions are catalyzed, with the diol-to-epoxide ratio apparently dependent on ligand topology and the spin state of the metal center. Herein we report further studies that demonstrate the sensitivity of the olefin oxidation reaction to the nature and topology of the tetradentate N4 ligand, revealing a complex reaction surface that appears to involve more than one type of metal-based oxidant.

Results and Discussion

Structural and spectroscopic characterization of iron(II) complexes containing linear N_2Py_2 ligands: The bpmen ligand serves as the prototype of a family of linear tetradentate N4 ligands that can in principle wrap around an iron center in three different topologies (Scheme 1).[16,17] Table 1 compares data from previously published structures of this family as well as from new structures reported herein. For bpmen, there is crystallographic evidence for only the *cis*-α topology.[18,19,20,21] This is exemplified by the structure of low-spin $[Fe^{II}(bpmen)(CH_3CN)_2](ClO_4)_2$ (**6**), in which the *N*-methyl groups are oriented *anti* with respect to each other. In solution, the complex exhibits a low-spin/high-spin equilibrium, but the C_2 symmetry of the complex is maintained, as indicated by NMR spectroscopy.[21,22] In contrast, the closely related bpmcn ligand can form two isomeric iron complexes with the *cis*-α (**7**) and the *cis*-β (**8**) topology, as illustrated by the crystal structures of $[Fe^{II}(\alpha\text{-bpmcn})(OTf)_2]$ (**7**)[23] and the closely related $[Fe^{II}(\beta\text{-5-Me}_2\text{-bpmcn})(OTf)_2]$ (**8′**).[24] In these structures, the *N*-methyl groups are oriented *anti* with respect to each other in the *cis*-α topology and *syn* with respect to each other in the *cis*-β topology. No interchange between *cis*-α and *cis*-β isomers of $[Fe^{II}(bpmcn)(OTf)_2]$ is observed in solution by NMR spectroscopy even at 50 °C in CD_3CN.[25] Such an interchange would entail epimerization at a tertiary amine that would require prior cleavage of the Fe–N bond.

The remaining topology not represented in the bpmen family until very recently[26,27] is the *trans* topology, with all four ligating atoms of the tetradentate N4 ligand approximately arrayed in the equatorial plane. To fill this gap, we initially designed the L^8py_2 ligand,[26] in which two propylene straps connecting the two 2-pyridylmethylamine units serve to enforce the desired topology. In the recently reported structure of $[Fe^{II}(L^8py_2)(OTf)](OTf)$ (**9**), the iron center in fact adopts a square-pyramidal arrangement with only one bound triflate occupying the apical position, leaving a free coordination site *trans* to the triflate anion.

To complete the comparisons within the bpmen ligand family, we investigated the iron coordination chemistry of bpmpn, a ligand with only one propylene strap connecting the two 2-pyridylmethylamine units. The bpmpn ligand appears to be more flexible than the other ligands in this family and gives rise to complexes with all three possible topologies (Table 1). Furthermore, unlike for the other ligands, interconversion between com-

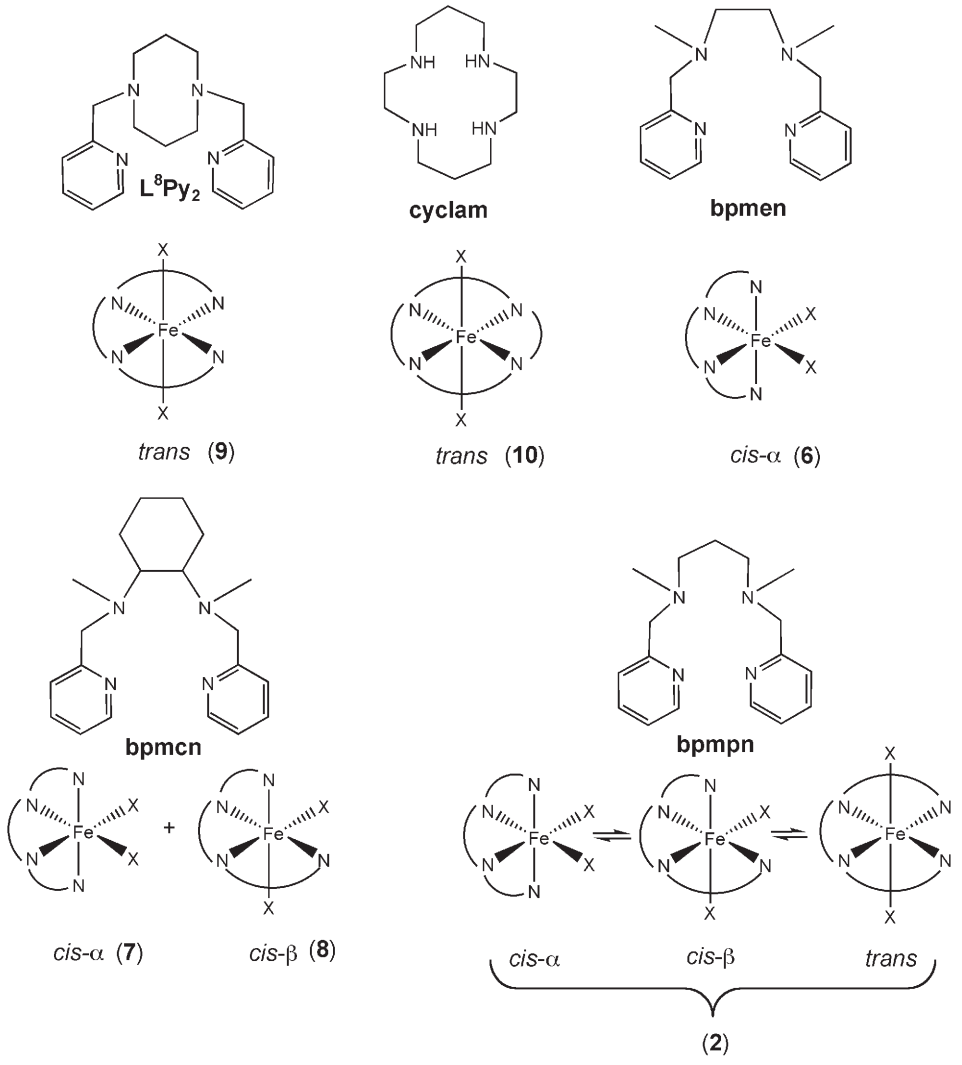

Scheme 1. Linear N4 ligands and topologies observed for their iron(II) complexes.

Table 1. Selected bond lengths [Å] and angles [°] for $[Fe^{II}(L)X_n]$ complexes.

Complex number	**1**	**2**	**3**	**4**	**5′**	**6**	**7**	**8′**	**9**
L	bpmpn	bpmpn	bpmpn	bpmpn	bpmpn	bpmen	bpmcn	5-Me_2-bpmcn	L^8Py_2
X	2 Cl	2 OTf	CH_3CN H_2O	1 Cl	OTf acetone	2 CH_3CN	2 OTf	2 OTf	1 OTf
topology	*cis*-α	*trans*	*cis*-β	tbp[a]	*trans*	*cis*-α	*cis*-α	*cis*-β	sp[b]
relative disposition of methyl groups	*anti*	*syn*	*anti*	*syn*	*syn*	*anti*	*anti*	*syn*	–
$Fe-N_{amine}$	2.365 2.365	2.218 2.237	2.204 2.209	2.221 2.174	2.231 2.229	2.055 2.053	2.220 2.237	2.239 2.203	2.216 2.176
$Fe-N_{pyridine}$	2.187 2.187	2.172 2.206	2.189 2.209	2.179 2.108	2.201 2.213	2.015 2.002	2.151 2.162	2.273 2.191	2.137 2.164
$Fe-N_{acetonitrile}$	–	–	2.211	–	–	1.941 1.950	–	–	–
$Fe-O_{(X)}$	–	2.126 2.128	2.111	–	2.093 (OTf) 2.183 (acetone)	–	2.131 2.159	2.083 2.190	2.011
Fe–Cl	2.448 2.448	–	–	2.277	–	–	–	–	–
N_{py}-Fe-N_{py}	162.40	111.45	99.34	96.05	112.26	176.53	175.49	102.02	109.73
X-Fe-X′	94.69	177.78	81.14	–	173.34	89.67	95.18	86.28	–
Ref.	[19]	[c]	[c]	[c]	[c]	[21]	[24]	[23]	[26]

[a] tbp = trigonal bipyramidal. [b] sp = square pyramidal. [c] This work.

plexes of different topologies is surprisingly facile (vide infra).

Previously published data on $[Fe(bpmpn)Cl_2]$ (**1**) show that the complex has a six-coordinate structure wherein the tetradentate ligand adopts a *cis*-α conformation.[18] The two chloride ligands are *cis* to each other, the two pyridine rings are coordinated *trans* to each other, and the relative disposition of the *N*-methyl groups is *anti*. The reaction of bpmpn with iron(II) salts of more weakly coordinating anions, namely $[Fe(CH_3CN)_2(OTf)_2]$ in CH_2Cl_2 and $Fe(ClO_4)_2{\cdot}6H_2O$ in CH_3CN led to the isolation of complexes $[Fe(bpmpn)(OTf)_2]$ (**2**) or $[Fe(bpmpn)(CH_3CN)(H_2O)](ClO_4)_2$ (**3**), respectively. In the crystal structure of **2** (Figure 1) the bpmpn ligand adopts a *trans* topology with the *N*-methyl groups *syn* relative to each other and the triflate ligands *trans* to each other. The two axial $Fe-O_{triflate}$ distances in **2** are essentially identical, suggesting that the sole propylene strap does not impose a distortion on the six-coordinate iron center. In the crystal structure of **3**, the bpmpn ligand adopts instead a *cis*-β topology where the two remaining coordination sites are occupied by CH_3CN and H_2O. Interestingly, unlike those of $[Fe^{II}(β\text{-}5\text{-}Me_2\text{-}bpmcn)(OTf)_2]$,[24] the *N*-methyl groups of **3** are *anti* with respect to each other, an arrangement that was previously observed for $[(bpmpn)Fe^{III}(Cl)(\mu\text{-}O)Fe^{III}Cl_3]$.[28] Thus, the ligand bpmpn can adopt the three possible topologies around an iron(II) center in octahedral complexes of the general formula $[FeN_4X_2]$, with the observed geometries strongly dependent on the nature of the X ligands.

Despite having different ligand topologies, bpmpn complexes **1**–**3** can be readily interconverted in solution at room temperature. For example, as shown in Scheme 2, treatment of **1** (*cis*-α) with two equivalents of silver triflate gives rise to **2** (*trans*) when the reaction is carried out in CH_2Cl_2 and to **3** (*cis*-β) when the reaction is carried out in CH_3CN (water ligand in **3** presumably derives from residual water present in CH_3CN solvent). Furthermore, **2** also converts to **3** when **2** is dissolved in CH_3CN. Lastly, both **2** and **3** revert to **1** by the addition of two equivalents of tetrabutylammonium chloride. The product iron complexes obtained by these procedures are readily identified by their characteristic ^1H NMR patterns, which are identical to those associated with the complexes obtained by direct synthesis. Although the observed changes in ligand topology may be construed as a shift of one pyridine from one site on an octahedron to an adjacent site, the associated change in the relative orientations of the *N*-methyl groups is not so simple and requires a facile mechanism for the epimerization of the *N*-methyl groups.

The observed facile interconversion among the three complexes suggests that more than one isomer is present in solutions of **2** and **3**. Indeed, evidence for the coexistence and interconversion of the three possible topological isomers of **2** is provided by variable-temperature ^{19}F NMR studies in CD_2Cl_2 (Figure 2). At ambient temperature, there are two very broad features at $\delta = -4$ and -46 ppm (FWHM ~3950 and 5080 Hz, respectively). As the temperature is decreased, these features sharpen and resolve into six signals at $-70\,^\circ C$. Set **2a** consists of a pair of peaks at $\delta = 23.7$ and -62.2 ppm of comparably large intensity, while set **2b** represents another pair of peaks at $\delta = 20.9$ and 12.7 ppm of smaller but comparable intensity. The remaining two peaks, also of low intensity, appear at $\delta = -5.9$ and -74.6 ppm. Sets **2a** and **2b** correspond to species containing two nonequivalent fluorine nuclei, consistent with complexes having *trans* or *cis*-β topologies. The ^1H NMR spectrum of this solution at $-70\,^\circ C$ shows that the major species in solution has only eight paramagnetically shifted resonances indicative of a symmetric species in which two halves of the molecule are related by means of a symmetry operation, thereby assigning set **2a** signals to the *trans* isomer. Set **2b** signals must then correspond to a minor isomer with *cis*-β topology. Since both *trans*- and *cis*-β topologies have *syn* *N*-methyl groups, this isomerization entails a simple shift of a pyridine to an adjacent site.

The low intensity signal at $\delta = -74.6$ ppm is quite broad and has a chemical shift that corresponds to free triflate. This assignment is confirmed by the addition of 0.3 or 2.5 equivalents of tetrabutylammonium triflate to CD_2Cl_2 solu-

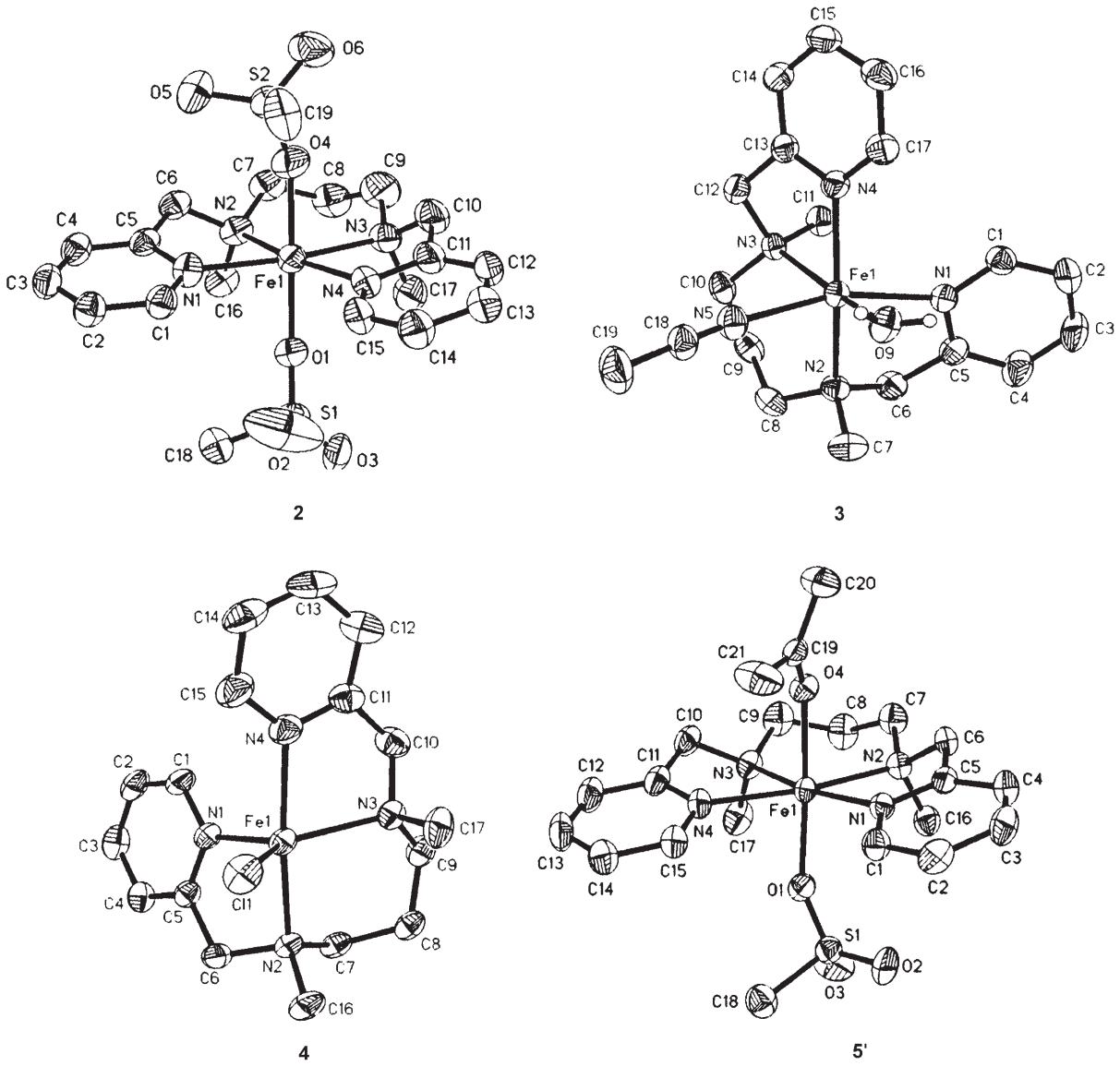

Figure 1. ORTEP representations of the structures of complexes **2**, **3**, **4**, and **5′**, showing 50% probability thermal ellipsoids. Hydrogen and fluorine atoms have been omitted for clarity.

tions of **2**, resulting in a proportionate increase in intensity. The appearance of free triflate suggests the dissociation of a triflate from the six-coordinate [Fe(bpmpn)$(OTf)_2$] complexes to form a five-coordinate species $[Fe(bpmpn)(OTf)]^+$.

To ascertain the NMR properties of such a five-coordinate species, we employed the synthetic strategy outlined in Scheme 3 to obtain a five-coordinate bpmpn complex. Complex [Fe(bpmpn)Cl]OTf (**4**) was obtained by the reaction of **2** with one equivalent of tetrabutylammonium chloride or by the reaction of [Fe(bpmpn)Cl_2] with one equivalent of silver triflate. The synthesis of **4** was established by ESI-MS (major peak at m/z 375.1 corresponding to the $[Fe(bpmpn)Cl]^+$ ion), ^{1}H and ^{19}F NMR spectroscopy, and X-ray diffraction. Its solid-state structure (Figure 1) shows a five-coordinate high-spin iron(II) center (d(Fe–N) $\approx$2.2 Å) bound to a tetradentate bpmpn ligand and a chloride, with the triflate being a non-coordinated counterion. The iron center is essentially trigonal bipyramidal having a τ value of 0.85 with the N2(amine)-Fe-N4(pyridine) as the largest angle (167.4°). In this structure the *N*-methyl groups of the bpmpn ligand have a *syn* relative disposition. Its ^{1}H NMR spectrum in CD_2Cl_2 at room temperature indicates an asymmetric coordination environment around the high-spin Fe^{II} center showing at least 15 different resonances in the range from $\delta = 110$ to -60 ppm. ^{19}F NMR measurements at room temperature show a broad band centered at $\delta = -62$ ppm with a bandwidth of about 760 Hz, suggesting an equilibrium between the five-coordinate species **4** and the six-coordinate species [Fe(bpmpn)Cl(OTf)].

Reaction with one equivalent of $AgSbF_6$ converts **4** to [Fe(bpmpn)(OTf)]SbF_6 (**5**), as indicated by ESI-MS (major peak at m/z 489.2 corresponding to the $[Fe(bpmpn)(OTf)]^+$

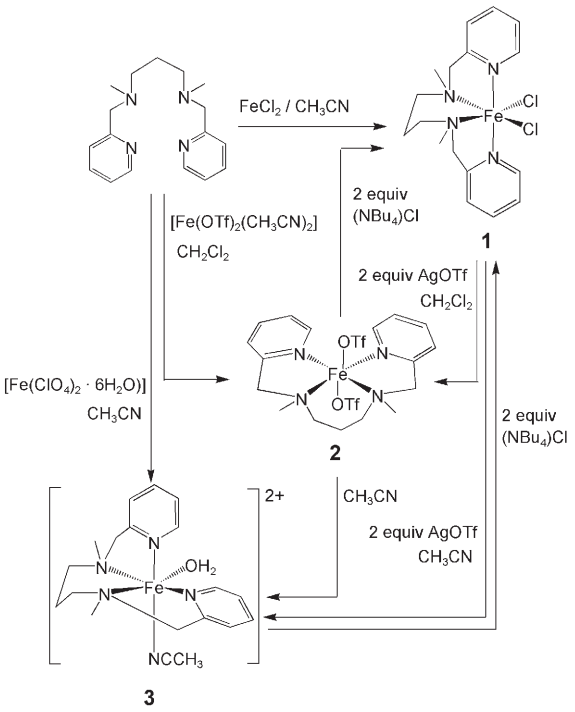

Scheme 2. Synthesis and interconversion of complexes **1**, **2**, and **3**.

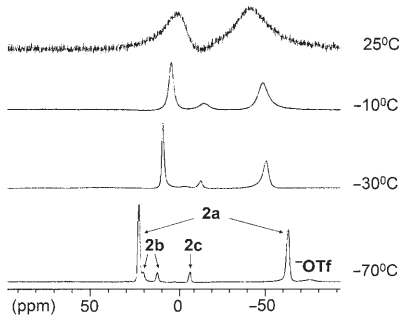

Figure 2. Variable-temperature ^{19}F NMR studies of a CH_2Cl_2 solution of **2**.

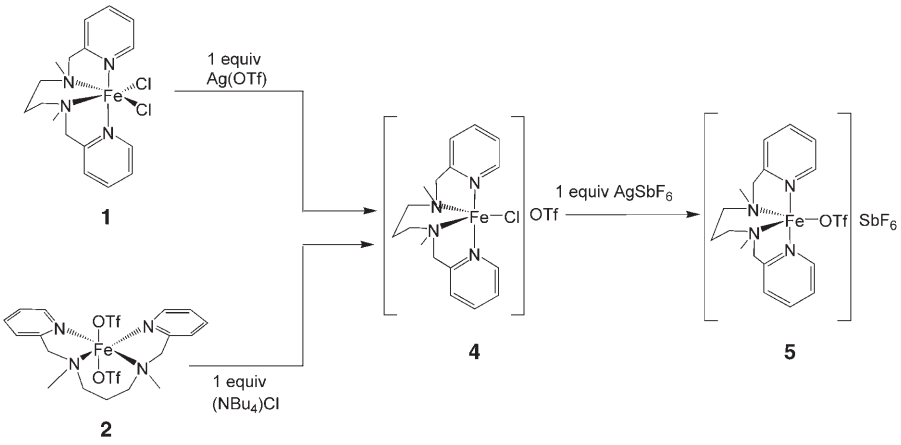

Scheme 3. Synthetic strategy to obtain complex **5**.

ion) and by ^{1}H and ^{19}F NMR spectroscopy. A sample of **5** recrystallized from acetone/diethyl ether affords crystals of $[Fe(bpmpn)(OTf)(CH_3COCH_3)]SbF_6$ (**5′**), in which one molecule of acetone is coordinated *trans* to the triflate ligand (Figure 1). The bpmpn ligand adopts a *trans* topology, as in **2**, and the *N*-methyl groups are disposed *syn* relative to each other. The ^{1}H NMR spectrum in CD_2Cl_2 of **5** at room temperature exhibits seven broad peaks in the range from $\delta =$ 150 to -40 ppm, indicative of a dynamic exchange undergone by this complex. ^{19}F NMR measurements confirm the fluxional behavior of **5** in CD_2Cl_2 at room temperature, showing a very broad signal (from $\delta = 20$ to -5 ppm) corresponding to coordinated triflate. However, at $-70\,^\circ$C the ^{19}F NMR spectrum of **5** displays seven different broad signals in the range from $\delta = 10$ to 110 ppm. These results indicate that **5** undergoes a dynamic interconversion among different isomers that are presumably the precursors for *cis*-α, *cis*-β, and *trans* structures, including isomers with a *syn* or *anti* relative disposition of the methyl groups of the bpmpn ligand. Additional possible isomers of **5** include diiron species similar to that recently reported for a $[(N_4Fe(OTf))_2(\mu\text{-}OTf)_2]$ complex.[29]

The observation of a free triflate signal in the low-temperature NMR spectrum of **2** requires that the pentacoordinate $[Fe(bpmpn)(OTf)]^+$ be present in this solution. However, none of the signals observed in the ^{19}F NMR spectrum of **5** at low temperature appears in that of **2**. Considering that the signal assigned to free triflate in the spectrum of **2** is broad and of low intensity, the signal pattern corresponding to $[Fe(bpmpn)(OTf)]^+$ dispersed over a range from 10 to 110 ppm may be of too low intensity to be detected. This leaves the remaining unassigned sharp singlet at $\delta = -5.9$ ppm in the low-temperature ^{19}F NMR spectrum of **2**, which can then be reasonably assigned to the two chemically equivalent triflates of the *cis*-α isomer.

Taken together, the NMR data reported above indicate that complex **2** in CH_2Cl_2 undergoes dynamic interconversion among isomers with *cis*-α, *cis*-β, and *trans* topologies by formation of pentacoordinate $[Fe(bpmpn)(OTf)]^+$ intermediate species, as represented in Scheme 4. These equilibria entail epimerization of the methyl groups of the bound bpmpn ligand, which requires the breaking of an Fe–N(amine) bond at some stage of the process. The occurrence of this dynamic process contrasts the situation for closely related $[Fe(bpmcn)(X)_2]$ complexes that can adopt both *cis*-α and *cis*-β topologies but do not interconvert in solution even at 50 °C in CD_3CN.[25] Perhaps even more curious is the fact that $[Fe(bpmen)(X)_2]$ complexes have so far only been found to adopt the *cis*-α topol-

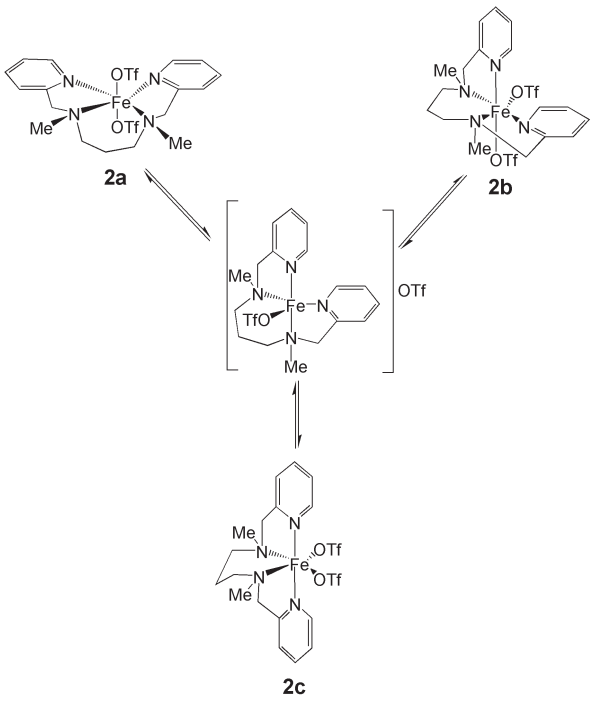

Scheme 4. Spontaneous interconversion of *cis*-α, *cis*-β, and *trans* isomers of **2** in CH_2Cl_2.

ogy. Thus, the fluxional behavior observed for the [Fe(bpmpn)$(OTf)_2$] complex is a unique feature of the bpmpn ligand.

The fluxional behavior of [Fe(bpmpn)$(OTf)_2$] in solution indicates a greater lability of the bpmpn ligand in comparison to bpmen or bpmcn. Unlike the latter two, bpmpn forms a six-membered [FeN_2C_3] ring upon binding to the iron center, which may result in a lower coordination affinity. This increase of the labilty of the bpmpn ligand also accounts for the easy replacement of the iron by silver when an excess of Ag^+ is added. This displacement is only observed for [Fe(bpmpn)$(OTf)_2$], but not for the analogous bpmen complex.

Since the catalysis experiments to be described below are usually carried out in acetonitrile, in which the coordinated triflate anions are displaced by solvent molecules, we studied the behavior of **3** in this solvent. Owing to the fact that the coordination sites occupied by triflate ions in **2** are occupied by solvent molecules in **3**, useful information can not be obtained from ^{19}F NMR spectroscopy. Thus, ^1H NMR spectroscopy has been the spectroscopic technique used to obtain a qualitative description of the behavior of **3** in solution. In CD_3CN, **3** exhibits at room temperature a paramagnetically shifted ^1H NMR spectrum with 11 signals in a range from $\delta = 150$ to -120 ppm. This pattern, which cannot be attributed solely to a pure *trans*, *cis*-α, or *cis*-β isomer, becomes even more complicated at $-40\,^\circ C$ where the corresponding spectrum exhibits at least 22 different signals in the range from $\delta = 170$ to -150 ppm. These observations indicate that a fast spontaneous isomerization also occurs for **3** in CH_3CN and give support to the interpretation proposed for the behavior observed in CH_2Cl_2 by means of ^{19}F NMR spectroscopy. That is, not only the simple exchange of triflate anions occurs in solution but also interconversion among the three different possible isomers of [Fe^{II}(bpmpn)$(OTf)_2$] is feasible at room temperature. This phenomenon may be responsible for the significant differences between the catalytic behavior of **2** and those observed for related [N_4FeX_2] complexes.

Catalytic behavior as a function of topology: The different possible topologies associated with the coordination of a linear N4 ligand to an octahedral Fe^{II} center result in significant variations in the chemical environments of the remaining coordination sites (Scheme 1) where activation of the H_2O_2 oxidant must take place. In the *trans* topology the two labile sites are *trans* to each other, limiting the potential cooperation between the two sites. However, in the *cis*-α and *cis*-β topologies, the two labile sites are *cis* with respect to each other, allowing the possibility for a cooperative interaction between these sites during catalysis. In the *cis*-α topology the two labile sites are chemically equivalent, being both *trans* to an aliphatic amine-nitrogen atom of the linear N_2Py_2 ligand, while in the *cis*-β topology the two labile sites are inequivalent, being *trans* to an aliphatic amine and a pyridine, respectively. Overall, the three topologies give rise to distinct chemical properties of the *cis*-α, *cis*-β, and *trans* isomers of a [$Fe(N_2Py_2)(L)_2$] catalyst. This notion was initially illustrated by the different catalytic behaviors of the *cis*-α and *cis*-β isomers of the [Fe(bpmcn)$(OTf)_2$] catalyst.[25] Now, we extend this comparison of catalytic behavior to other members of the linear N_2Py_2 family (Scheme 1), including a complex (**9**) that is constrained to have a *trans* topology (Table 2). Here we present a systematic study of six complexes that includes the effects of temperature and added water on their catalytic behavior (Figures 3 and 4, Tables 2 and 4) as well as ^{18}O-labeling experiments (Table 3). The effect of added water has been investigated because such conditions are necessary for ^{18}O-labeling experiments that have proven so useful in providing mechanistic insight.[14,15] Commercially available $H_2{}^{18}O_2$ is typically a 2% solution in water, so the use of 10 equivalents of $H_2{}^{18}O_2$ entails concomitant addition of approximately 1000 equivalents of H_2O.

The mechanistic framework within which the results of these experiments are evaluated is shown in Scheme 5 and mainly derives from detailed studies of [Fe(tpa)] catalysis.[14] This framework postulates the activation of H_2O_2 by an iron(III) center with two *cis*-labile sites via either a non-water-assisted (*nwa*) pathway or a water-assisted (*wa*) pathway. There is strong indirect evidence for the *wa* pathway in [Fe(tpa)] catalysis, as both epoxide and *cis*-diol incorporate label from $H_2{}^{18}O$ into the products. It is proposed that water incorporation occurs via an $HO{-}Fe^V{=}O$ oxidant that is formed through a water-assisted cleavage of the O–O bond of an $H_2O{-}Fe^{III}{-}OOH$ intermediate. The *nwa* pathway must be invoked to account for the lack of label incorporation from $H_2{}^{18}O$ into the products for some members of the [Fe-

Table 2. Catalytic efficiency of nonheme iron catalysts towards olefin oxidation at room temperature.

Ligand	cyclam	L^8Py_2	bpmen	bpmcn	bpmcn		bpmpn
Complex number	**10**	**9**	**6**	**7**	**8**	**7 + 8**	**2**
Topology	*trans*	*trans*	*cis*-α[a]	*cis*-α[b]	*cis*-β[b]		
cyclooctene							
diol + epoxide (TN)[c]	3.5	3.9	8.4	6.5	7.7	7.4	6.0
[diol]/[epoxide]	0.03	0.1	0.1	0.1	1.8	0.6	0.7
1-octene							
diol + epoxide (TN)[c]	1.7	1.0	5.4	6.4	4.7	4.1	4.1
[diol]/[epoxide]	0.2	0.3	0.3	0.2	2.1	0.6	3.8
cis-2-heptene							
diol + epoxide (TN)[c]	4.6	2.9	6.4	7.0	6.8		4.2
[diol]/[epoxide]	0.04	0.1	0.1	0.1	0.8		0.8
% RC[d] epoxide	93	83	92	>99	67		60
% RC[d] diol	>99	>99	79	>99	85		>99
trans-2-heptene							
diol + epoxide (TN)[c]	2.2	4.2	5.7	5.7	5.6		2.2
[diol]/[epoxide]	0.1	0.04	0.2	0.05	0.6		0.5
% RC[d] epoxide	>99	96	84	>99	86		88
% RC[d] diol	>99	>99	96	>99	81		>99

[a] Data from reference [14]. [b] Data from reference [25]. [c] TN = Turnover number. [d] % RC = 100 × (*cis* − *trans*)/(*cis* + *trans*).

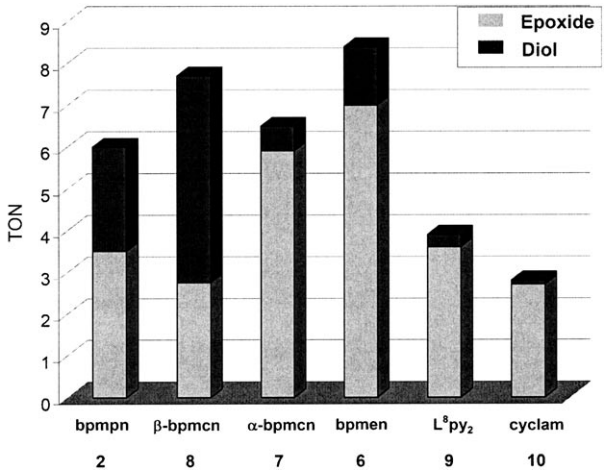

Figure 3. Product yields for the oxidation of cyclooctene with H_2O_2 catalyzed by nonheme iron complexes.

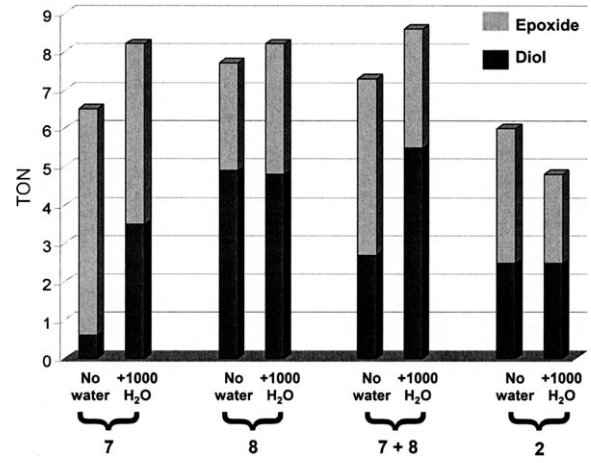

Figure 4. Effect of water addition in the oxidation of cyclooctene at room temperature with H_2O_2 catalyzed by complexes **7**, **8**, **7**+**8**, and **2**.

(tpa)] catalyst family and, according to the data presented below, may involve an Fe^{III}–η^2-OOH species. However, unlike $[Fe^{III}(tpa)(\eta^1\text{-OOH})]^{2+}$, this species has not been detected.

*trans Complexes **9** and **10***: Complex **9**, whose L^8Py_2 ligand is designed to maintain a *trans* topology in solution, exhibits a strong preference for epoxidation with high stereoselectivity, as does **10**, a complex of the macrocyclic ligand cyclam previously studied by Nam, Ho, and Valentine (see Figure 3).[30] Addition of 1000 equivalents of water reduces the activity of these complexes by 40–50%, suggesting that water may compete with H_2O_2 in coordinating the iron center (Table 4). Interestingly, there is a small amount of *cis*-diol (0.1–0.3 TON) that is obtained under normal conditions. The *cis*-diol product becomes undetectable when water is added or in experiments carried out at low temperature (−15 °C) with or without added water. It is not clear how the very minor *cis*-dihydroxylation product can be formed by a complex with *trans*-labile sites, as the nature of the reaction would appear to require two *cis*-labile sites. Access to a ligand arrangement that affords *cis*-labile sites has been shown to be possible for the cyclam ligand,[31,32,33] but this isomer is very likely thermodynamically much less favored.

Experiments in the presence of isotopically labeled $H_2{}^{18}O$ for the oxidation of cyclooctene catalyzed by **9** and **10** show

Table 3. ^{18}O-labeling results for cyclooctene oxidation by **2**, and **6**–**10** in CH_3CN.

		% ^{18}O-epoxide	% ^{18}O-diol		
			No ^{18}O	^{18}O–^{16}O	^{18}O–^{18}O
9	$H_2{}^{18}O_2$	60	–	–	–
	$H_2{}^{18}O$	<1	–	–	–
10	$H_2{}^{18}O_2$	88	–	–	–
	$H_2{}^{18}O$	<1	–	–	–
6[a]	$H_2{}^{18}O_2$	73	41	58	1
	$H_2{}^{18}O$	30	23	73	4
7[b]	$H_2{}^{18}O_2$	90	3	89	7
	$H_2{}^{18}O$	11	11	88	1
8[b]	$H_2{}^{18}O_2$	66	2	4	93
	$H_2{}^{18}O$	15	97	3	0
7 + 8	$H_2{}^{18}O_2$	57	2	4	94
	$H_2{}^{18}O$	16	96	4	0
2 (room temp)	$H_2{}^{18}O_2$	31	3	7	90
under air	$H_2{}^{18}O$	21	96	3	1
2 (room temp)	$H_2{}^{18}O_2$	70	0	4	96
under Ar	$H_2{}^{18}O$	31	97	2	1
2 (−40 °C)	$H_2{}^{18}O_2$	48	1	4	95
under air	$H_2{}^{18}O$	55	96	4	0

[a] Data from reference [34]. [b] Data from reference [25].

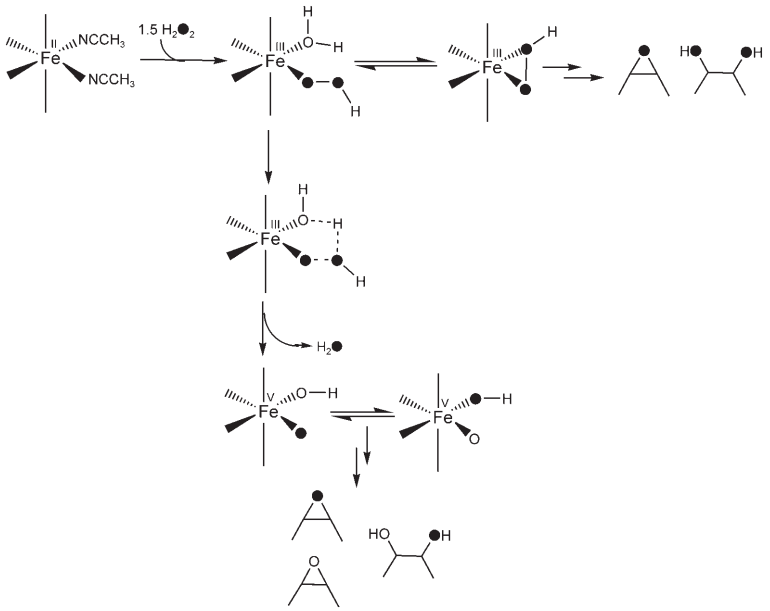

Scheme 5. Proposed mechanisms for oxidation of olefins with H_2O_2 catalyzed by non-heme iron complexes.

no incorporation of the labeled water into the epoxide product (Table 3). In addition, when $H_2{}^{18}O_2$ is used, the epoxide product shows only partial incorporation of the ^{18}O label, indicating some involvement of radical processes, particularly for **9**, that generate product with air oxidation. While these results clearly exclude a *wa* mechanism for the epoxidation, the nature of the active oxidizing species cannot be ascertained since no intermediate has been trapped in the reactions of either **9** or **10** with H_2O_2. The Fe^{III}–OOH intermediate proposed in the *nwa* pathway is a plausible candidate for **9**, as the related Fe^{III}–OOR species has been observed and characterized in its low-temperature reaction with *t*BuOOH.[26]

cis-α *Complexes* ***6*** *and* ***7***: Complexes with *cis*-α topology (**6** and **7**) are efficient catalysts for highly stereoselective olefin epoxidation with diol/epoxide (D/E) ratios of 0.1:1 (see Figure 3).[14,25] Under the same conditions, **6** and **7** generally afford about twice as much epoxide product as **9** and **10**, suggesting that the *cis*-α topology provides a superior ligand arrangement for activating H_2O_2 for epoxidation. However, as previously reported, the addition of 1000 equivalents of H_2O in cyclooctene oxidation experiments catalyzed by **6** increases the D/E ratio from 0.1:1 to 0.8:1, so *cis*-dihydroxylation becomes a more important reaction under these conditions.[34] Similarly, the addition of 1000 equivalents of H_2O to a cyclooctene oxidation experiment catalyzed by **7** increases the D/E ratio from 0.1:1 to 0.7:1 (see Figure 4). These observations suggest that different active species may be formed for complexes with *cis*-α topology depending on the presence or absence of water in the reaction media.

^{18}O-labeling experiments provide clues into the nature of the active species for olefin oxidation catalyzed by **6** or **7**. Consistent with our previous work on **6**, ^{18}O-labeling experiments for **7** show that the diol product incorporates one oxygen atom from H_2O_2 and one oxygen atom from water (Table 3), thereby strongly implicating a *wa* mechanism (Scheme 5). The epoxide product also incorporates some ^{18}O label from water, suggesting that the *wa* pathway also contributes to the epoxidation of cyclooctene. However the dramatic differences in the D/E ratios that depend on the presence of water suggest that a different active species is responsible for the chemistry in the absence of added water. Under the latter conditions, we propose that **6** and **7** follow a *nwa* pathway, in which the main active species is proposed to be LFe^{III}–OOH that affords epoxide as a main product.

Experiments at low temperature (−15 °C) were carried out to evaluate the relative energetics of the different pathways. In the absence of water, decreasing the temperature diminishes the turnover yield of **7** by a factor of 5. Adding 1000 equivalents of H_2O decreases this yield by another factor of 5. This comparison suggests that the *wa* mechanism has a higher activation barrier than the *nwa* pathway for catalysts with a *cis*-α topology.

cis-β *Complex* ***8***: In contrast to its *cis*-α isomer, **8** with a bpmcn ligand in a *cis*-β topology exhibits a marked preference for olefin *cis*-dihydroxylation, with a D/E ratio of 1.8:1 in the case of cyclooctene oxidation (see Figure 3).[25] Like its *cis*-α isomer, the epoxide product shows some amount of label incorporation from $H_2{}^{18}O$, consistent with the involvement of a *wa* pathway. Considering the fact that the two *cis* labile sites are not equivalent in the structure of **8**, one may expect that label scrambling in the HO–Fe^{V}=O species will not be complete, so the *wa* pathway could be the dominant mechanism for epoxidation. However, unlike for its *cis*-α isomer, the *cis*-diol product derives both oxygen atoms only from H_2O_2, strongly implicating a *nwa* pathway for *cis*-dihydroxylation. Within the constraints of the original mechanistic framework (Scheme 5), these observations suggest the generation of two different active species derived from **8**: one obtained through a *wa* mechanism responsible for epoxidation of cyclooctene and the other one obtained through a *nwa* pathway that accounts for *cis*-dihydroxylation.

In contrast to what is observed for **6** and **7**, the addition of water does not significantly affect the D/E ratio or the turnover yield for the reactions catalyzed by **8** at room temperature (see Figure 4). However, decreasing the reaction temperature to −15 °C nearly doubles the D/E ratio, indicat-

ing that the *cis*-dihydroxylation process is the kinetically preferred pathway. More interestingly, whereas the turnover yield drops by a factor of 5 upon going to −15 °C in the absence of added water, as observed for **7**, it is only halved in the presence of added water. So the addition of water in fact increases the activity of **8** nearly threefold at low temperature. These results are puzzling. The labeling experiments showing a *nwa* pathway for *cis*-dihydroxylation led us to the expectation that the diol yield should not be affected by the presence of water. So, it is not clear how addition of water can have a positive effect on the diol yield at lower temperature.

*Equimolar mixture of **7** and **8***: The different pathways and products derived from the reaction of **7** and **8** with H_2O_2 led us to investigate the oxidation of olefins with equimolar amounts of **7** and **8** (designated **7+8**) to assess their relative reactivities. Since **7** and **8** individually give rise to clearly different D/E ratios in olefin oxidation (see Figure 3), the distribution of oxidized products in these experiments should allow us to estimate the extent of *cis*-α or *cis*-β catalysis in olefin oxidation. For the oxidation of cyclooctene and 1-octene, the **7+8** combination affords D/E ratios of about 0.6:1 in the absence of added water, values intermediate between those observed for the individual *cis*-α or *cis*-β isomers, suggesting that the two isomers are comparably reactive. However, when the oxidation of cyclooctene is catalyzed by an equimolar mixture of **7** and **8** in the presence of added water, the product distribution resembles that for **8** alone (see Figure 4). Accordingly, labeling experiments (which necessarily require an excess of water) for **7+8** give results very close to those observed for **8** alone. A similar conclusion can be reached in experiments at −15 °C. Scrutiny of the data suggests that **7** is deactivated by the presence of water and **8** becomes the dominant catalyst under these conditions.

*Complex **2***: The chemistry of the bpmpn complex **2** provides an interesting twist to this study of topological effects, since **2** differs from the other complexes in consisting of a mixture of *cis*-α, *cis*-β, and *trans* isomers that can interconvert in solution, despite solid-state evidence for discrete topological isomers. Interestingly, the D/E ratios obtained using **2** generally resemble those observed for **8**, except for cyclooctene where autooxidation contributes significantly to the yield of epoxide (see Table 2). These observations suggest that the *cis*-β isomer is the more active form of **2** in acetonitrile. Consistent with that observed for **8**, labeling experiments show that both diol oxygen atoms come from H_2O_2 (see Table 3), which implicates a *nwa* mechanism for *cis*-dihydroxylation. However, labeling experiments show that cyclooctene oxide derives its oxygen 31% from $H_2{}^{18}O$ and 70% from $H_2{}^{18}O_2$ when the experiments are carried out under argon (see Table 3). (In air, the incorporation of ^{18}O in the epoxide product is 21% in the presence of $H_2{}^{18}O$ and 31% using $H_2{}^{18}O_2$, so the other half of the epoxide product arises from a radical autoxidation pathway.) So there appear to be, at least, two reactive species in the mixture that constitutes **2**: one derived from a *nwa* mechanism responsible for *cis*-dihydroxylation and the other from a *wa* pathway, responsible for epoxidation.

However **2** behaves differently from **7+8** when the temperature is lowered. At −15 °C, the D/E ratio decreases significantly, particularly in the presence of added water. So, unlike for **7+8**, *nwa* dihydroxylation is less favored than *wa* epoxidation. This conclusion is supported by labeling experiments at −40 °C where the diol product is formed by a *nwa* mechanism and the epoxide product, on the other hand, is formed solely by a *wa* mechanism, as it is 50% labeled by either $H_2{}^{18}O_2$ and $H_2{}^{18}O$ labeling data.

Mechanistic overview: Based on the observations presented above, the mechanistic landscape for the oxidation of olefins by nonheme iron catalysts appears to be not as simple as first described on the basis of detailed studies on the [Fe(tpa)] catalyst.[14,15] Ligand topology plays a large role, as demonstrated by complexes **6**–**10**. The complexes with *trans* (**9** and **10**) and *cis*-α (**6** and **7**) topologies strongly favor epoxidation via a *nwa* pathway. However for the *cis*-α catalysts, addition of water significantly changes the product ratio and gives rise to comparable amounts of epoxide and *cis*-diol. ^{18}O-labeling experiments attribute this change to a shift towards a *wa* pathway for both epoxidation and *cis*-dihydroxylation. These results are easily accommodated by the mechanistic framework presented in Scheme 5, in which the addition of water favors the proposed $H_2O{-}Fe^{III}{-}OOH$ aquated derivative from which is generated the $HO{-}Fe^{V}{=}O$ active species that effects both epoxidation and *cis*-dihydroxylation. Indeed DFT calculations on [Fe(bpmen)] (**6**) have found the activation barriers for O–O bond cleavage to differ by only 1 kcal mol^{-1} for the *nwa* and the *wa* pathways,[34] well within the margin of error ascribed to DFT calculations.

The experimental results obtained for **2** and **8** however complicate the original mechanistic framework. Complex **8** is the only one in our study with an established *cis*-β topology, while **2** consists of a mixture of isomers. Both **2** and **8** catalyze *cis*-dihydroxylation reactions that are not affected by the addition of water and found to occur solely via a *nwa* pathway. On the other hand, the incorporation of labeled water into epoxide products requires the involvement of a *wa* pathway that exclusively forms epoxide. Thus two distinct oxidizing agents must be formed. The presumed $HO{-}Fe^{V}{=}O$ oxidant formed in the *wa* pathways of **2** and **8** must differ from corresponding species associated with the *wa* pathways of **6**, **7**, and [Fe(tpa)], wherein the putative $HO{-}Fe^{V}{=}O$ oxidant affords comparable amounts of epoxide and *cis*-diol products. For the $[Fe^{V}(tpa)(O)(OH)]^{2+}$ intermediate, DFT calculations show that epoxidation and *cis*-dihydroxylation have comparable activation barriers with respective olefin attacks occurring at the oxo and hydroxo atoms.[35] However, given ligand backbones and topologies that are different from those of tpa, the activation barriers for epoxidation and *cis*-dihydroxylation do not necessarily have to be

isoenergetic. In fact, experimental results suggest that for **2** and **8** epoxidation is more favored than *cis*-dihydroxylation by the putative $[Fe^{V}(L)(O)(OH)]$ oxidant generated from a *wa* pathway. As a consequence a species different to $[Fe^{V}(L)(O)(OH)]$ should be proposed as responsible of the *nwa cis*-dihydroxylation. Within the proposed mechanistic framework it seems reasonable suggest that it is the $[Fe^{III}(\eta^2\text{-OOH})]$ species that accounts for generation of *cis*-diol.

The mechanistic picture we have described thus far presents a reaction surface that is quite sensitive to the specifics of the reaction. Comparative studies at 25 and −15 °C show that the relative activation barriers for the two possible reactions with and without added water are dependent on the nature of the N_2Py_2 ligand (Table 4). The *nwa* pathway is favored at lower temperature for **7** and **8**, affording predominantly epoxide product for **7** and *cis*-diol product for **8**. In a competition between **7** and **8**, the major product is the *cis*-diol formed by a *nwa* pathway, suggesting that the latter catalyst is more effective at lower temperature. On the other hand, the major product for **2** at lower temperature is the epoxide formed by a *wa* pathway, so just the insertion of an additional methylene group in the bridge that connects the two pyridylmethylamine halves of the tetradentate ligand is sufficient to affect significantly the relative energetics of the two reactions.

Table 4. Effect of water and temperature on $Fe(N_2Py_2)$ catalysts in cyclooctene oxidation in CH_3CN.

Catalyst	Temperature	25 °C		−15 °C	
	added water	0	1000 [equiv]	0	1000 [equiv]
9	diol + epoxide (TN)	3.9	1.9	1.7	1.5
	[diol]/[epoxide]	0.1	~0	~0	~0
10	diol + epoxide (TN)	3.5	2.1	2.3	1.5
	[diol]/[epoxide]	0.03	~0	~0	~0
7	diol + epoxide (TN)	6.5	8.2	1.7	0.2
	[diol]/[epoxide]	0.1	0.7	0.2	0.3
8	diol + epoxide (TN)	7.7	8.2	1.6	4.5
	[diol]/[epoxide]	1.8	1.4	2.9	3.0
7+8	diol + epoxide (TN)	7.4	8.6	1.7	3.5
	[diol]/[epoxide]	0.6	1.7	1.3	2.2
2	diol + epoxide (TN)	6.0	4.8	2.2	2.5
	[diol]/[epoxide]	0.7	1.1	0.2	0.08

Recently Nam and co-workers have reported experimental evidence that argues against $[Fe^{III}(OOH)]$ species as oxidants directly responsible for oxygen-atom transfer reactions.[36] They investigated the reactivities of the three $[Fe^{III}(L)(OOH)]^{2+}$ (L = tpa, N4Py, Bn-tpen) intermediates, all of which can be trapped at low temperature and characterized spectroscopically to be low-spin ($S = {}^1/_2$) iron(III) complexes, and found that the decay of these pre-formed intermediates is not accelerated by the addition of substrates. At first glance, these recent results may appear to undermine the mechanistic framework presented in Scheme 5 for the $[Fe(N_2Py_2)]$ catalysts that postulate $[Fe^{III}(\eta^2\text{-OOH})]$ or $[Fe^{V}(O)(OH)]$ species as oxidants. However, of the three iron(II) precursor complexes that give rise to $[Fe^{III}(L)(OOH)]^{2+}$ intermediates studied by Nam and co-workers, the two with pentadentate ligands (L = N4Py and Bn-tpen) are catalytically ineffective for olefin oxidation. This leaves [Fe(tpa)], which is an excellent and highly stereoselective catalyst for olefin oxidation like the $[Fe(N_2Py_2)]$ catalysts discussed in this paper.[14] Nam's conclusion does not contradict Scheme 5, as we have already reported compelling labeling results that exclude $[Fe^{III}(tpa)(OOH)]^{2+}$ as the oxidant. Instead we have postulated that it serves as the precursor to the actual $[Fe^{V}(O)(OH)]$ oxidant in the *wa* pathway. For the $[Fe(N_2Py_2)]$ catalysts discussed in this paper, corresponding $[Fe^{III}(L)(OOH)]^{2+}$ intermediates have to date not been observed. Perhaps these do not exist or they are simply too reactive to be trapped. In the absence of evidence to the contrary, the putative $[Fe^{III}(L)(\eta^2\text{-OOH})]^{2+}$ oxidants remain the best candidates to account for the *cis*-dihydroxylation of olefins by the *nwa* pathway. This mechanistic notion is supported by the crystallographic observation of a side-on bound dioxygen ligand in the iron active site of naphthalene dioxygenase[10] as well as DFT calculations on the arene *cis*-dihydroxylation reaction catalyzed by this enzyme.[37]

Experimental Section

Materials and methods: All reagents were purchased from Aldrich and used as received unless noted otherwise. CH_3CN and CH_2Cl_2 solvents were distilled over CaH_2 before use. $H_2{}^{18}O_2$ (90% ^{18}O-enriched, 2% solution in $H_2{}^{16}O$) was obtained from Cambridge Isotope Lab., and $H_2{}^{18}O$ (95% ^{18}O-enriched) was received from ICON isotop. The *cis*- and *trans*-2-heptenes were purified by passing through silica gel immediately before the reactions. The syntheses of all metal complexes were carried out in a glove box under a dry N_2 atmosphere. The syntheses of $[Fe^{II}(bpmen)(OTf)_2]$ and $[Fe^{II}(L_8py_2)(OTf)_2]$ followed procedures previously reported.[21,26] ^1H NMR, ^{19}F NMR, and ^{13}C NMR spectra were recorded on a Varian Unity 300 or 500 spectrometer. ^1H and ^{13}C chemical shifts (ppm) were referenced to the residual solvent peaks. ^{19}F chemical shifts were referenced to an $CFCl_3$ external reference. Electrospray ionization mass spectral experiments were carried out on a Bruker BioTOF II mass spectrometer using the following conditions: spray chamber voltage = 4000 V; gas carrier temperature = 200 °C. Samples for ESI-MS analysis were prepared in a CH_3CN/H_2O 1:1 mixture. Product analyses were performed on a Perkin-Elmer Sigma 3 gas chromatograph (AT-1701 column, 30 m) with a flame ionization detector. GC mass spectral analyses were performed on a HP 5898 GC (DB-5 column, 60 m) with a Finnigan MAT 95 mass detector or a HP 6890 GC (HP-5 column, 30 m) with an Agilent 5973 mass detector. A 4% NH_3/CH_4 mix was used as the ionization gas for chemical ionization analyses.

[Fe(bpmpn)(OTf)$_2$] (2): A solution of bpmpn (0.300 g, 1.05 mmol) ligand in CH_2Cl_2 (5 mL) was added to a suspension of $[Fe(CH_3CN)_2(OTf)_2]$ (0.457 g, 1.05 mmol) in CH_2Cl_2.(5 mL). The reaction mixture was stirred for 3 h at room temperature and the resulting solution filtered. Solid product **2** was obtained by concentrating the filtrate to 5 mL and adding water until precipitation. The precipitate was filtered off and washed with ether. Recrystallization was carried out in CH_2Cl_2/diethyl ether at room temperature. Yield: 345 mg (51%). This procedure led to the isolation of diffraction-quality crystals. Both amorphous and crystalline products are hygroscopic. Elemental analysis indicate that, during manipulation, crystals of **2** incorporate one molecule of water for each molecule of iron complex. Elemental analysis calcd (%) for $C_{19}H_{24}F_6FeN_4O_6S_2\cdot H_2O$

(**2**): C 34.75, H 3.94, N 8.53, S 9.75; found: C 34.88, H 3.77, N 8.42, S 9.73.

[Fe(bpmpn)(CH_3CN)(H_2O)](ClO_4)$_2$ (3): Solid $Fe(ClO_4)_2\cdot 6H_2O$ (0.382 g, 1.05 mmol) was added to a solution of bpmpn (0.300 g, 1.05 mmol) in CH_3CN (15 mL). The reaction mixture was stirred for 3 h at room temperature. The reaction mixture was then filtered to remove insoluble inorganic salts, and then concentrated to 5 mL. Addition of diethyl ether led to the separation of **3** as an oil, which converted to an hydroscopyc brown solid after being subject to vacuum over 5 h. This solid was washed several times with diethyl ether before recrystallization from diethyl ether/CH_3CN. X-ray quality crystals of [(bpmpn)Fe(CH_3CN)(H_2O)](ClO_4)$_2$ were obtained by this method. Yield: 260 mg (41 %). Elemental analysis calcd (%) for $C_{19}H_{29}Cl_2FeN_5O_9\cdot H_2O$ ([(bpmpn)Fe(CH_3CN)(H_2O)](ClO_4)$_2\cdot H_2O$ (**3**)): C 37.01, H 5.03, N 11.36; found: C 37.06, H 4.91, N 11.42.

[Fe(bpmpn)Cl]OTf (4): Silver triflate (125.5 mg, 0.486 mmol) was added to a solution of [Fe(bpmpn)Cl_2] (0.200 g, 0.486 mmol) in CH_2Cl_2 (10 mL). The suspension was stirred for 6 h at room temperature until complete precipitation of AgCl, which was removed by filtration. Product **4** was obtained by adding diethyl ether to the previously concentrated (to 5 mL) filtrate. X-ray quality crystals were obtained by crystallization from CH_2Cl_2/diethyl ether. Yield: 210 mg (82 %). Elemental analysis calcd (%) $C_{18}H_{24}ClF_3FeN_4O_3S$ (**4**): C 41.18, H 4.57, N 10.67, S 6.10; found: C 41.23, H 4.19, N 10.60, S 6.07.

Alternative synthesis of **4**: Treatment of **2** (0.300 g, 0.47 mmol) in CH_2Cl_2 (10 mL) with $[N(Bu)_4]Cl$ (0.130 g, 0.47 mmol). The suspension was stirred for 4 h, and after that time filtered and concentrated to 5 mL. Compound **4** was obtained as a yellow solid after addition of diethyl ether. Yield: 141 mg (57 %). Addition of an excess of AgOTf (>2 equivalents) to a solution of **1** affords a white solid that can be identified as [Ag(bpmpn)](OTf) by ESI-MS (*m*/*z* 391, corresponding to $[Ag(bpmpn)]^+$).

[Fe(bpmpn)(OTf)]SbF_6 (5): An equimolar amount of $AgSbF_6$ (0.100 g, 0.29 mmol) was added to a solution of product **4** (0.150 g, 0.29 mmol) in CH_2Cl_2 (10 mL). After the mixture had been stirred for 3 h, the AgCl formed was removed by filtration, and the resulting solution concentrated to 5 mL. Complex **5** was precipitated by adding diethyl ether to the concentrated solution. The solid obtained was washed several times with diethyl ether. Yield: 188 mg (89 %). Elemental analysis calcd (%) for $C_{18}H_{24}F_9FeN_4O_3SSb$ (**5**): C 29.80, H 3.31, N 7.73, S 4.42; found: C 29.97, H 3.42, N 7.76, S 4.36. X-ray quality crystals were obtained from recrystallization in CH_2Cl_2/acetone. The found structure corresponds to the formula **5**$\cdot CH_3C(O)CH_3$ (**5′**).

[Fe(cyclam)(CH_3CN)$_2$](ClO_4)$_2$ (10): Solid $Fe(ClO_4)_2\cdot 6H_2O$ (0.363 g, 1.0 mmol) was added to a solution of cyclam (0.200 g, 1.0 mmol) in CH_3CN (10 mL), and reaction mixture was stirred for 6 h at room temperature. After this time **5** appeared as a purple solid, which was isolated by filtration. The solid obtained was washed several times with small portions of CH_3CN and with diethyl ether. Yield: 333 mg (62 %). Elemental analysis calcd (%) for $C_{14}H_{30}Cl_2FeN_6O_8$ (**5**)**:** C 31.28, H 5.58, N 15.64; found: C 31.37, H 5.71, N 15.55.

Crystallographic studies

The structures were solved at the X-ray Crystallographic Laboratory of the Chemistry Department of the University of Minnesota. A crystal of complex **2**, **3**, **4**, or **5′** was placed onto the tip of a 0.1-mm diameter glass capillary and mounted on a CCD area detector diffractometer for a data collection at 173(2) K. A preliminary set of cell constants was calculated from reflections harvested from three sets of 20 frames. These initial sets of frames were oriented such that orthogonal wedges of reciprocal space were surveyed. The data collection was carried out using $Mo_{K\alpha}$ radiation (graphite monochromator) with a frame time of 45 s and a detector distance of 4.9 cm. A randomly oriented region of reciprocal space was surveyed to the extent of one sphere and to a resolution of 0.84 Å. Four major sections of frames were collected with 0.30° steps in ω at four different φ settings and a detector position of −28° in 2θ. The intensity data were corrected for absorption and decay (SADABS).[38] Final cell constants were calculated from the actual data collection after integration (SAINT).[39] Pertinent crystallographic data and experimental conditions are summarized in Table 5. Structures were solved and refined using Bruker SHELXTL.[40] The space groups were determined based on systematic absences and intensity statistics. A direct-methods solution was calculated which provided most non-hydrogen atoms from the E-map. Full-matrix least squares/difference Fourier cycles were performed which located the remaining non-hydrogen atoms. All non-hydrogen atoms were refined with anisotropic displacement parameters. All hydrogen atoms were placed in ideal positions and refined as riding atoms with relative isotropic displacement parameters.

Table 5. Crystallographic data and structural refinement details for compounds **2**, **3**, **4** and **5′**.

	2	**3**	**4**	**5′**
formula	$C_{19}H_{24}F_6FeN_4O_6S_2$	$C_{21}H_{32}Cl_2FeN_6O_9$	$C_{18}H_{24}ClF_3FeN_4O_3S$	$C_{21}H_{30}F_9FeN_4O_4SSb$
M_r	638.39	639.28	524.77	783.15
crystal system	monoclinic	triclinic	triclinic	monoclinic
space group	$P2_1/n$	$P\bar{1}$	$P1$	$P2_1/c$
a [Å]	13.687(2)	9.5552(11)	8.9605(11)	9.7261(13)
b [Å]	11.893(2)	12.0468(13)	9.3177(11)	21.476(3)
c [Å]	16.813(3)	13.8233(15)	13.8028(17)	14.875(2)
α [°]	90	72.447(2)	86.142	90
β [°]	111.066(2)	79.665	84.883(2)	108.254
γ [°]	90	74.174(2)	88.599(2)	90
V [Å^3]	2553.9(7)	1451.4(3)	1145.0(2)	2950.9(7)
Z	4	2	2	4
T [K]	173(2)	173(2)	173(2)	173(2)
λ [Å]	0.71073	0.71073	0.71073	0.71073
ρ [g cm^{-3}]	1.660	1.463	1.522	1.763
μ [cm^{-1}]	8.41	7.60	9.17	15.69
independent reflections	4519	6604	4052	6043
goodness-of-fit	1.078	1.036	1.047	1.081
$R1$[a] [$I>2(I)$]	0.0529	0.0358	0.0493	0.0478
$wR2$[b] [$I>2(I)$]	0.1317	0.0932	0.1266	0.0934

[a] $R1=||F_o|-|F_c||/|F_o|$. [b] $wR2=\{[w(F_o^2-F_c^2)^2]/[w(F_o^2)^2]\}^{1/2}$.

CCDC-284391 (**5′**), CCDC-284392 (**4**), CCDC-284393 (**3**), CCDC-284394 (**2**) contain the supplementary crystallographic data for this paper. These data can be obtained free of charge from The Cambridge Crystallographic Data Centre via www.ccdc.cam.ac.uk/data_request/cif.

Reaction conditions for catalytic oxidations: Catalytic oxidations were carried out as reported elsewhere.[14] 0.3 mL of a 70 mM H_2O_2 solution (diluted from a 35 or 50 % H_2O_2 solution) in CH_3CN was delivered by syringe pump over 30 min at 25 °C in air to a CH_3CN solution (2.7 mL) containing iron catalyst and olefin substrate. The final concentrations were 0.7 mM mononuclear iron catalyst, 7.0 mM H_2O_2, and 0.70 M olefin. For competition experiment the final concentration of α-[Fe(bpmcn)(OTf)$_2$] and β-[Fe(bpmcn)(OTf)$_2$] was 0.35 mM. The solution was stirred for another 5 min after syringe pump addition was complete. The resulting solutions were treated with acetic anhydride (1 mL) together with 1-methylimidazole (0.1 mL) to esterify the diol products. Organic products were extracted with $CHCl_3$. To the organic extract was added naphthalene as an internal standard and the solution was subjected to GC analysis. The products were identified by comparison of their GC retention

times. All experiments were run at least in duplicate, the reported data being the average of these reactions.

Isotope labeling studies: Variations from the conditions described above are the following: In experiments with $H_2{}^{18}O$, 42 μL of $H_2{}^{18}O$ (70 mM, 1000 equivalents) was added to the catalyst solution prior to the injection of H_2O_2. In experiments with $H_2{}^{18}O_2$, 7.0 mM $H_2{}^{18}O_2$ (diluted by CH_3CN from a 2% $H_2{}^{18}O_2/H_2O$ solution) was used instead of H_2O_2. The organic products were subjected to GC/CI-MS analyses.

Acknowledgements

This work was supported by a grant from the U.S. Department of Energy (FFG02–03ER15455 to L.Q.). R.M. thanks the Ministerio de Educación y Ciencia of Spain for postdoctoral support. The authors would like to acknowledge the efforts of Benjamin E. Kucera and Dr. Victor G. Young, Jr. of the X-Ray Crystallographic Laboratory, Department of Chemistry, University of Minnesota in solving the crystal structures reported.

[1] M. Costas, M. P. Mehn, M. P. Jensen, L. Que Jr., *Chem. Rev.* **2004**, *104*, 939.
[2] D. T. Gibson, V. Subramanian, in *Microbial Degradation of Organic Compounds* (Ed.: D. T. Gibson), Marcel Dekker, New York, **1984**, pp. 181.
[3] P P. R. Ortiz de Montellano, *Cytochrome P-450 Structure, Mechanism and Biochemistry*, 2nd ed., Plenum, New York, **1995**.
[4] W. Nam, "Cytochrome P-450" in *Comprehensive Coordination Chemistry II*, *Vol. 8*, (Volume Eds.: L. Que, Jr., W. B. Tolman, Series Eds.: J. McCleverty, T. J. Meyer), Elsevier, Amsterdam, **2004**, p. 281.
[5] I. G. Denisov, T. M. Makris, S. G. Sligar, I. Schlichting, *Chem. Rev.* **2005**, *105*, 2253.
[6] F. A. Walker, *Chem. Rev.* **2004**, *104*, 589.
[7] H. Fujii, *Coord. Chem. Rev.* **2002**, *226*, 51.
[8] E. Y. Tshuva, S. J. Lippard, *Chem. Rev.* **2004**, *104*, 987–1012.
[9] B. Kauppi, K. Lee, E. Carredano, R. E. Parales, D. T. Gibson, H. Eklund, S. Ramaswamy, *Structure* **1998**, *6*, 571.
[10] A. Karlsson, J. V. Parales, R. E. Parales, D. T. Gibson, H. Eklund, S. Ramaswamy, *Science* **2003**, *299*, 1039.
[11] M. D. Wolfe, J. V. Parales, D. T. Gibson, J. D. Lipscomb, *J. Biol. Chem.* **2001**, *276*, 1945.
[12] D. T. Gibson, R. E. Parales, *Curr. Opin. Biotechnol.* **2000**, *11*, 236.
[13] K. D. Koehntop, J. P. Emerson, L. Que Jr., *J. Biol. Inorg. Chem.* **2005**, *10*, 87.
[14] K. Chen, M. Costas, J. Kim, A. K. Tipton, L. Que Jr., *J. Am. Chem. Soc.* **2002**, *124*, 3026.
[15] K. Chen, M. Costas, L. Que Jr., *J. Chem. Soc. Dalton Trans.* **2002**, 672.
[16] J. R. Aldrich-Wright, R. S. Vagg, P. A. Williams, *Coord. Chem. Rev.* **1997**, *166*, 361.
[17] U. Knof, A. von Zelewsky, *Angew. Chem.* **1999**, *111*, 312; *Angew. Chem. Int. Ed.* **1999**, *38*, 302.
[18] S. Taktak, S. V. Kryatov, E. V. Rybak-Akimova, *Inorg. Chem.* **2004**, *43*, 7196.
[19] N. Raffard, V. Balland, J. Simaan, S. Létard, M. Nierlich, K. Miki, F. Banse, E. Anxolabéhère-Mallart, J.-J. Girerd, *C. R. Chim.* **2002**, *5*, 99.
[20] P. Mialane, L. Tchertanov, F. Banse, J. Sainton, J.-J. Girerd, *Inorg. Chem.* **2000**, *39*, 2440.
[21] K. Chen, L. Que Jr., *Chem. Commun.* **1999**, 1375.
[22] K. P. Bryliakov, E. A. Duban, E. P. Talsi, *Eur. J. Inorg. Chem.* **2005**, *1*, 72.
[23] M. Costas, J.-U. Rohde, A. Stubna, R. Y. N. Ho, L. Quaroni, E. Münck, L. Que Jr., *J. Am. Chem. Soc.* **2001**, *123*, 12931.
[24] M. Costas, A. K. Tipton, K. Chen, D.-H. Jo, L. Que Jr., *J. Am. Chem. Soc.* **2001**, *123*, 6722.
[25] M. Costas, L. Que Jr., *Angew. Chem.* **2002**, *114*, 2283; *Angew. Chem. Int. Ed.* **2002**, *41*, 2179.
[26] M. R. Bukowski , H. L. Halfen, T. A. van den Berg , J. A. Halfen, L. Que Jr., *Angew. Chem.* **2005**, *117*, 590; *Angew. Chem. Int. Ed.* **2005**, *44*, 584.
[27] G. J. P. Britovsek, J. England, A. J. P. White, *Dalton Trans.* **2006**, 1399.
[28] N. Raffard, F. Banse, K. Miki, M. Nierlich, J.-J. Girerd, *Eur. J. Inorg. Chem.* **2002**, 1941.
[29] M. P. Jensen, S. J. Lange, M. P. Mehn, E. L. Que, L. Que Jr., *J. Am. Chem. Soc.* **2003**, *125*, 2113.
[30] W. Nam, R. Ho, J. S. Valentine, *J. Am. Chem. Soc.* **1991**, *113*, 7052.
[31] R. Guilard, O. Siri, A. Tabard, G. Broeker, P. Richard, D. J. Nurco, K. J. Smith, *J. Chem. Soc. Dalton Trans.* **1997**, 3459.
[32] K. Meyer, E. Bill, B. Mienert, T. Weyhermuller, K. Weighardt, *J. Am. Chem. Soc.* **1999**, *121*, 4859.
[33] H. Chun, E. Bill, E. Bothe, T. Weyhermuller, K. Weighardt, *Inorg. Chem.* **2002**, *41*, 5091.
[34] D. Quiñonero, K. Morokuma, D. G. Musaev, R. Mas-Ballesté, L. Que Jr., *J. Am. Chem. Soc.* **2005**, *127*, 6548.
[35] A. Bassan, M. R. A. Blomberg, P. E. M. Siegbahn, L. Que Jr., *Angew. Chem.* **2005**, *117*, 2999; *Angew. Chem. Int. Ed.* **2005**, *44*, 2939.
[36] M. J. Park, J. Lee, Y. Suh, J. Kim W. Nam, *J. Am. Chem. Soc.* **2006**, *128*, 2630.
[37] A. Bassan, M. R. A. Blomberg, P. E. M. Siegbahn, *J. Biol. Inorg. Chem.* **2004**, *9*, 439.
[38] R. Blessing, *Acta Crystallogr. Sect. A* **1995**, *51*, 33–38.
[39] SAINT V6.2, Bruker Analytical X-Ray Systems, Madison, WI (2001).
[40] SHELXTL V6.10, Bruker Analytical X-Ray Systems, Madison, WI (2000).

Received: April 1, 2006
Published online: July 26, 2006

